R-matrix method for quantum transport simulations in discrete systems

Gennady Mil'nikov,* Nobuya Mori, and Yoshinari Kamakura
Graduate School of Engineering, Osaka University, 2-1 Yamada-oka, Suita, Osaka 565-0871, Japan
(Received 29 April 2009; revised manuscript received 4 June 2009; published 29 June 2009)

We present a discrete analog of the *R*-matrix method for atomistic quantum transport calculations. The method enables all the observables of interest to be found recursively and the computer time scales linearly with the number of atoms regardless of the device geometry, distribution of impurities, or interface roughness.

DOI: 10.1103/PhysRevB.79.235337 PACS number(s): 73.23.−b, 73.40.Qv

I. INTRODUCTION

Semiconductor process technologies are making rapid progress in terms of device scale and performance. Nanofabrication is being achieved as a result of continual technological innovations, leading to the development of a variety of novel devices such as double gate transistors,[1] carbon nanotubes,[2] and gate-all-around (GAA) metal oxide semiconductor field effect transistors (MOSFETs).[3] Experimental studies of Ge/Si nanowire heterostructures and GAA twin silicon nanowire have shown excellent gate control, high drain current, and reduced sensitivity to temperature. As the size of a CMOS shrinks, a device cannot longer be described as a continuous system with smooth boundaries and interfaces. Atomic-scale variation in the dopant distribution and the interface roughness must be taken into account, necessitating statistical quantum simulations of nanoscale MOSFETs. In order to turn theoretical studies into a practical computer design tool, improvements in efficiency of the theoretical methods are still needed. A variety of methods, such as the contact block reduction (CBR) algorithm,[4,5] scattering matrix approach,[6,7] and recursive Green's function method[8] have been developed to calculate ballistic transport through quantum devices. However, even in the ballistic regime, the large size of the Hamiltonian makes computations in three-dimensional nanostructures very challenging.[9]

For continuous models, we have shown recently that the electronic state of the device can be effectively calculated in a local basis representation.[10] The local basis is introduced by splitting the device into a set of small elements and solving an independent low-dimensional spectral problem in each element. Constructing the device from its elements is equivalent to calculating the normal derivatives of the Green's function (or the wave function) at their boundaries which play a role of unknown parameters in the local basis representation. The continuity at the internal boundaries provides necessary consistency conditions which are conveniently expressed in terms of the *R* matrix.[11,12] The latter serves as an auxiliary quantity which can be propagated through the device such that the physical solutions in the device elements are constructed recursively without huge operations. Unlike the recursive Green's function method, the propagated *R* matrix characterizes a close device without leads and the propagation scheme can be adjusted for arbitrary device geometry. Apart from its numerical efficiency, the method provides a suitable framework for studying ionized impurity scattering and screening effects since the singularities in the charge distribution can be handled analytically in appropriate local coordinate representation. Calculations of quantum transport through dopant atoms in semiconductor nanowire have been reported recently.[13]

In the continuous models, the *R* matrix is originally defined via a linear relation between the scattering wave function and its normal derivative at the contacts with leads. An alternative definition arises naturally in scope of the local basis representation: the *R* matrix for any device element is merely a boundary projection of the Green's function for appropriately chosen close system.[10] The later definition can be easily adopted to discrete models and the *R*-matrix theory is formulated in much the same way taking the device elements as arbitrary clusters of atoms. In practice, using individual atoms as the device elements gives the best computer performance in the ballistic regime and offers a natural way to incorporate random impurity distribution and/or surface roughness.

II. TRANSPORT IN TIGHT-BINDING MODEL

A. Green's functions and the *R* matrix

We consider the tight-binding Hamiltonian in space of atomic orthogonal pseudo-orbitals

$$\mathbf{H}_{\mathrm{tot}} = \begin{pmatrix} \mathbf{H}_{DD} & \mathbf{H}_{DL} \\ \mathbf{H}_{LD} & \mathbf{H}_{LL} \end{pmatrix}, \tag{1}$$

where $\mathbf{H}_{DD}$ is the Hamiltonian of the device, $\mathbf{H}_{LL}$ represents the Hamiltonian of all the leads, and $\mathbf{H}_{DL}=\mathbf{H}_{LD}^{+}$ is the coupling between the device and the leads. The interatomic coupling in $\mathbf{H}_{\mathrm{tot}}$ is assumed to be localized, i.e., each atom in the structure interacts with a finite number of neighbors. In particular, the coupling term $\mathbf{H}_{DL}$ is nonzero only for a small number of atoms in the device (D) and leads (L) near the contacts. We express this condition in the form $\mathbf{H}_{DL}=P\mathbf{H}_{DL}P'$, where $P=P^2$ ($P'=P'^2$) is the projector to the corresponding atomic orbitals in the device (leads). In the ballistic regime, all the physical observables can be obtained from the retarded Green's function of the device

$$\mathbf{G}_{DD}^{R}(\varepsilon) = (\varepsilon - \mathbf{H}_{\mathrm{tot}} + i0)_{DD}^{-1} = [\varepsilon - \mathbf{H}_{DD} - \mathbf{\Sigma}^{R}(\varepsilon)]^{-1}, \tag{2}$$

where the self-energy

$$\mathbf{\Sigma}^{R}(\varepsilon) \equiv \mathbf{H}_{DL}(\varepsilon - \mathbf{H}_{LL} + i0)^{-1}\mathbf{H}_{LD} \tag{3}$$

represents the effects of the leads. The Green's function $(\varepsilon - \mathbf{H}_{LL} + i0)^{-1}$ is calculated routinely from the Bloch scattering

 ©2009 The American Physical Society

solutions in the leads.[14] Since the coupling part of the Hamiltonian is localized, the rank of $\mathbf{\Sigma}^R = P\mathbf{\Sigma}^R P$ depends only on the number of atoms at the contacts which is much smaller then in the whole device. As a result, in the representation where $\mathbf{H}_{DD}$ is diagonal, the calculation of the device Green's function $\mathbf{G}^R_{DD}(\varepsilon)$ can be reduced to a few matrix operations of small size, which is the essence of the CBR method.[5]

The same results most easily follow from the Dyson equation

$$\mathbf{G}_{DD}(\varepsilon) = \mathbf{G}_0(\varepsilon)(1 + \mathbf{H}_{DL}\mathbf{G}_{LD}), \tag{4}$$

where $\mathbf{G}_0(\varepsilon) = \frac{1}{\varepsilon - \mathbf{H}_{DD}}$ is the Green's function for the close device with the Hamiltonian $\mathbf{H}_{DD}$. The retarded Green's function is a particular solution of Eq. (4) which behaves as outgoing/decaying Bloch waves in all the leads. We follow the common approach and consider the leads of nanowire geometry with the slice index $s=0,1,2,\ldots$ along the wire and the zeroth slice taken as the contact. We introduce the matrix $\boldsymbol{\chi}_s$ of all the outgoing/decaying solutions in all the leads.[14,15] In practice, $\boldsymbol{\chi}_s$ is block diagonal, the blocks for separate leads are calculated independently. It is also assumed that the Hamiltonian couples only the nearest slices. Then the projector P (P') corresponds to the atomic orbitals in the zeroth (first) slice and the retarded Green's function satisfies the condition that $P\mathbf{G}^R_{DD}$ and $P'\mathbf{G}^R_{LD}$ are linear combinations of $\boldsymbol{\chi}_0$ and $\boldsymbol{\chi}_1$ with the same expansion coefficients. We thus obtain

$$P'\mathbf{G}^R_{LD} = \boldsymbol{\chi}_1\boldsymbol{\chi}_0^{-1}P\mathbf{G}^R_{DD}, \tag{5}$$

which after inserting into Eq. (4) gives the ordinary Dyson equation for the retarded Green's function[16]

$$\mathbf{G}^R(\varepsilon) = \mathbf{G}_0(\varepsilon)(1 + \mathbf{\Sigma}^R\mathbf{G}^R) \tag{6}$$

with the contact self-energy

$$\mathbf{\Sigma}^R = P\mathbf{H}_{DL}\boldsymbol{\chi}_1\boldsymbol{\chi}_0^{-1}P. \tag{7}$$

Hereafter we consider only the device area and omit the indices D in the Green's function. In the leads with equivalent slices $\boldsymbol{\chi}_1 = \boldsymbol{\chi}_0\mathbf{Z}$ and $\mathbf{\Sigma}^R = P\mathbf{H}_{DL}\boldsymbol{\chi}_0\mathbf{Z}\boldsymbol{\chi}_0^{-1}P$, where $\mathbf{Z}$ is the matrix of the corresponding Bloch factors.[16] This is generally not the case in realistic structures and Eq. (7) should be used.

In the ballistic regime, calculation of the entire $\mathbf{G}^R(\varepsilon)$ can be avoided. In particular, the current between leads i and j is expressed in terms of the transmission function[16]

$$T_{ij}(\varepsilon) = \mathrm{Tr}\,\mathbf{\Gamma}_i\mathbf{G}^R\mathbf{\Gamma}_j\mathbf{G}^{R+}, \tag{8}$$

where

$$\mathbf{\Gamma}_i = i(\mathbf{\Sigma}^R_i - \mathbf{\Sigma}^{R+}_i) \tag{9}$$

and $\mathbf{\Sigma}^R_i$ is the part of the self-energy for the ith lead. As follows from Eq. (7), the Green's function $\mathbf{G}^R$ in Eq. (8) can be replaced by $P\mathbf{G}^R P$ and Eq. (6) gives

$$P\mathbf{G}^R P = \mathbf{R}(\mathbf{1} - \mathbf{\Sigma}^R\mathbf{R})^{-1}, \tag{10}$$

where we introduced the R matrix $\mathbf{R}$ as a boundary projection of the Green's function for the close device

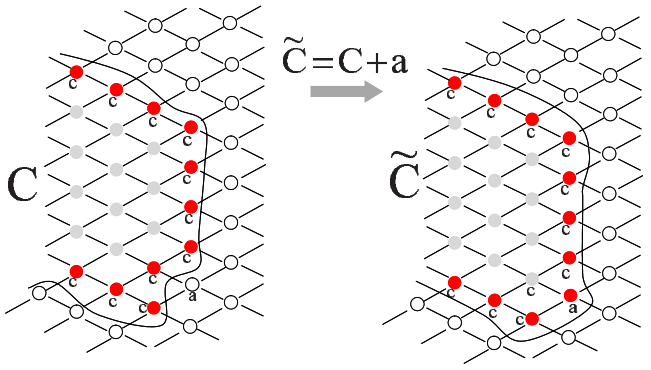

FIG. 1. (Color online) The device growth: the new cluster $\tilde{C}$ is obtained by adding atom a to the previous cluster C. The red (dark gray) circles represent the atoms in the cluster boundary. The light gray circles are for other atoms in the clusters. The projector P_c in Eq. (12) extracts the atomic orbitals at the boundary atoms c. After adding the new atom, $P_{\tilde{c}}$ in Eq. (20) removes the orbitals of $c \cup a$, which are not in the boundary of the new cluster $\tilde{C}$ (one c atom in this case).

$$\mathbf{R} = P\mathbf{G}_0 P. \tag{11}$$

Rather than calculate the Green's function $\mathbf{G}_0$, we will directly construct the R matrix and avoid any huge operations depending on the size of the total device.

B. Device growth and the *R*-matrix propagation

Let C be an arbitrary cluster of atoms in the device area and let $B \equiv D - C$ be the rest of the device. We define the cluster boundary c as a group of all the atoms in C with $H_{CB} \neq 0$ and introduce the projector operators $P_c, P_C, P_B, \ldots$ onto atomic orbitals of $c, C, B, \ldots$. Similar to Eq. (11), we can introduce the close system with the Hamiltonian $\mathbf{H}_{CC} \equiv P_C\mathbf{H}_{\mathrm{tot}}P_C$ and define the corresponding R matrix

$$\mathbf{R}_{cc} \equiv P_c\frac{1}{\varepsilon - \mathbf{H}_{CC}}P_c, \tag{12}$$

which is simply a boundary block of the Green's function for the isolated cluster C (i.e., without coupling $\mathbf{H}_{CB}$). Figure 1 schematically shows a part of cluster C and its boundary atoms c. The R matrix $\mathbf{R}_{cc}$ gives a linear relation between arbitrary wave function at these atoms $\Psi_c \equiv P_c\Psi(\varepsilon)$ and the exterior of the cluster $\Psi_B \equiv P_B\Psi(\varepsilon)$ (empty circles in Fig. 1),

$$\Psi_c = \mathbf{R}_{cc}\mathbf{H}_{cB}\Psi_B. \tag{13}$$

We can now increase the cluster by adding an arbitrary atom $a \in B$ (see Fig. 1),

$$C \to \tilde{C} = C + a,$$

$$B \to \tilde{B} = B - a, \tag{14}$$

and write for the wave function at $c \cup a$,

$$\Psi_c = \mathbf{R}_{cc}\mathbf{H}_{ca}\Psi_a + \mathbf{R}_{cc}\mathbf{H}_{c\tilde{B}}\Psi_{\tilde{B}}, \tag{15}$$

$$\Psi_a = \mathbf{R}_{aa}\mathbf{H}_{ac}\Psi_c + \mathbf{R}_{aa}\mathbf{H}_{a\tilde{B}}\Psi_{\tilde{B}}, \tag{16}$$

where $\mathbf{R}_{aa} \equiv \frac{1}{\varepsilon - \mathbf{H}_{aa}}$ is the Green's function for the isolated atom with the Hamiltonian $\mathbf{H}_{aa}$. Performing necessary matrix operation, we arrive at

$$\begin{pmatrix} \Psi_c \\ \Psi_a \end{pmatrix} = \begin{pmatrix} \tilde{\mathbf{R}}_{cc} & \tilde{\mathbf{R}}_{ca} \\ \tilde{\mathbf{R}}_{ac} & \tilde{\mathbf{R}}_{aa} \end{pmatrix} \begin{pmatrix} \mathbf{H}_{c\tilde{B}}\Psi_{\tilde{B}} \\ \mathbf{H}_{a\tilde{B}}\Psi_{\tilde{B}} \end{pmatrix}, \tag{17}$$

where

$$\tilde{\mathbf{R}}_{cc} = \mathbf{R}_{cc} + \mathbf{R}_{cc}\mathbf{H}_{ca}(1_{aa} - \mathbf{R}_{aa}\mathbf{H}_{ac}\mathbf{R}_{cc}\mathbf{H}_{ca})^{-1}\mathbf{R}_{aa}\mathbf{H}_{ac}\mathbf{R}_{cc},$$

$$\tilde{\mathbf{R}}_{ca} = \mathbf{R}_{cc}\mathbf{H}_{ca}(1_{aa} - \mathbf{R}_{aa}\mathbf{H}_{ac}\mathbf{R}_{cc}\mathbf{H}_{ca})^{-1}\mathbf{R}_{aa},$$

$$\tilde{\mathbf{R}}_{ac} = (1_{aa} - \mathbf{R}_{aa}\mathbf{H}_{ac}\mathbf{R}_{cc}\mathbf{H}_{ca})^{-1}\mathbf{R}_{aa}\mathbf{H}_{ac}\mathbf{R}_{cc},$$

$$\tilde{\mathbf{R}}_{aa} = (1_{aa} - \mathbf{R}_{aa}\mathbf{H}_{ac}\mathbf{R}_{cc}\mathbf{H}_{ca})^{-1}\mathbf{R}_{aa}. \tag{18}$$

Similar to Eq. (13), $\tilde{\mathbf{R}}_{(c\cup a)(c\cup a)}$ in the above equation is a projection of the Green's function for close cluster $\tilde{C}$ to the boundary of C and to the new atom a. Since any boundary atom of the new cluster $\tilde{C}$ is within this group,

$$P_{\tilde{c}}(P_c + P_a) = (P_c + P_a)P_{\tilde{c}} = P_{\tilde{c}} \tag{19}$$

we obtain the R matrix for the grown cluster $\tilde{C}$ by simply removing redundant orbitals $\notin \tilde{c}$,

$$\mathbf{R}_{\tilde{c}\tilde{c}} = P_{\tilde{c}}\tilde{\mathbf{R}}_{(c\cup a)(c\cup a)}P_{\tilde{c}}. \tag{20}$$

Equations (18) and (20) give the general recipe of the atomistic R-matrix propagation. We can now start with the initial R matrix R_{aa} for arbitrary isolated atom and construct the device by adding all other atoms one by one. Note that Eq. (18) preserves the hermicity of the R matrix and involves only the coupling $\mathbf{H}_{ca}$ with the last atom. In particular, the size of the inversion operation in Eq. (18) is just the number of the atomic orbitals N_{orb} at a. Thus, calculating the R matrix at one energy point requires $\sim N_b^2 N_{orb}^3 N_D$ operations in total, where N_D is the number of atoms in the device and N_b is a typical number of atoms at cluster boundaries. The latter depends on the consecutive order of atoms in the device growth. In practice, one can always minimize the boundary and keep N_b to be on the order of the number of atoms at the contacts.

C. Example: *R*-matrix propagation in Si *T* junction

As an illustration, we calculate the transmission function in silicon T junction [Fig. 2(a)] in scope of the sp^3s^* tight-binding model.[17] Surface states of the device are eliminated by the method of Ref. 18. In order to test the numerical accuracy, we first compare the R-matrix propagation with the direct diagonalization of the close system Hamiltonian in the device with short ~0.5 nm straight sections (1024 atoms in total). We have confirmed at least 11 significant digits of accuracy in all the elements of the final R matrix. Figure 3 presents the transmission functions $T_{12}(\varepsilon), T_{13}(\varepsilon)$ for the energies within the valence band of the leads. For comparison we show on the same picture the transmission function $T_0(\varepsilon)$ in the [100] ideal wire of the same cross section. In these calculations the length of the straight sections of the T junction varied up to 10 nm with 7872 atoms in total. The transmission functions are found to be independent on the length with accuracy better than ten significant digits in the whole energy interval. The calculations were repeated for the device with a vacancy in the central area [see Fig. 2(a)] and similar accuracy has been found. Since a single step of the R-matrix propagation does not involve any large computer operation, there are no memory limitations on the device size.

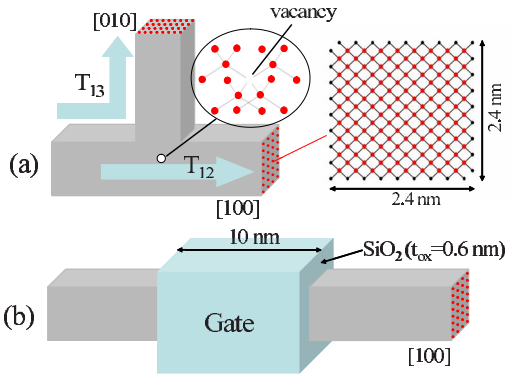

FIG. 2. (Color online) T junction and GAA MOSFET used in the simulations. Si-wire cross section: small black dots represent outer hydrogen sites.

III. CARRIER DENSITY AND SELF-CONSISTENT CALCULATION OF QUANTUM TRANSPORT

We proceed with calculating the carrier charge[16]

$$q_a = \pm 2(\text{for spin})e\sum_i \int \frac{d\varepsilon}{2\pi} f_i(\varepsilon)\text{Tr}_a[\mathbf{G}^R\mathbf{\Gamma}_i\mathbf{G}^{R^+}], \tag{21}$$

where i runs over all the leads, the sign and the Fermi factors f_i depend on the carrier type, and Tr_a is taken over atomic

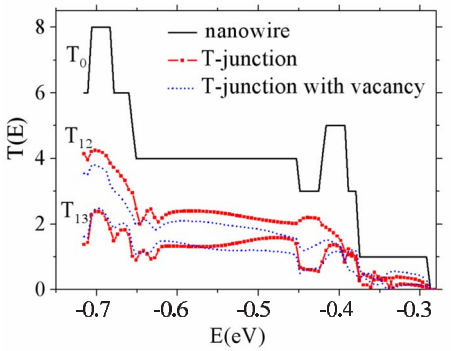

FIG. 3. (Color online) The transmission functions T_{12} and T_{13} of the T junction in Fig. 2(a) with and without a vacancy in the central region of the device. For comparison, the transmission function T_0 of the ideal [100] nanowire is also shown.

orbitals at atom a. Introducing the open-channel eigenfunctions

$$\mathbf{\Gamma}_i|i\nu\rangle = \Lambda_{i\nu}|i\nu\rangle, \tag{22}$$

we rewrite Eq. (21) in the form

$$q_a = \pm 2e\sum_{i\nu}\int \frac{d\varepsilon}{2\pi} f_i(\varepsilon)\langle\Psi_a(i\nu)|\Psi_a(i\nu)\rangle, \tag{23}$$

where the scattering wave function

$$\Psi(i\nu) = \mathbf{G}^R P|i\nu\rangle\sqrt{\Lambda_{i\nu}} \tag{24}$$

can be calculated at all the atoms recursively.

To see this, we again consider cluster $\tilde{C}$ obtained by adding atom a to the previous cluster C. According to Eq. (17), any wave function at a is related to the exterior of $\tilde{C}$ by

$$\Psi_a = \Theta_{a\tilde{B}}\Psi_{\tilde{B}}, \tag{25}$$

where

$$\Theta_{a\tilde{B}} = \tilde{\mathbf{R}}_{ac}\mathbf{H}_{c\tilde{B}} + \tilde{\mathbf{R}}_{aa}\mathbf{H}_{a\tilde{B}}. \tag{26}$$

Note that only atoms $\tilde{b}\in\tilde{B}$ with $\mathbf{H}_{\tilde{c}\tilde{b}}\neq 0$ actually contribute to Eq. (25). The small coupling matrix $\Theta_{a\tilde{b}}$ of size $\sim N_b N_{orb}^2$ can be stored in the course of the R-matrix propagation. Thus, for known $\Psi_{\tilde{b}}$ the wave function at the previously added atom Ψ_a is calculated trivially. Subtracting atom a gives the previous cluster C. Since any atom $b\in B$ with $\mathbf{H}_{cb}\neq 0$ is within $\tilde{b}\cup a$ we can repeat the same operation for the last atom in C which was added right before a. In this way, any wave function can be successively calculated at all the atoms in the reverse order which requires only $N_b N_{orb}^2$ operations at each atom. The initial conditions for the backward propagation are specified at the contacts. For the wave function Eq. (24) we obtain from Eq. (10)

$$P\Psi(i\nu) = \mathbf{R}(1-\Sigma^R\mathbf{R})^{-1}|i\nu\rangle\sqrt{\Lambda_{i\nu}} \tag{27}$$

with the R matrix $\mathbf{R}$ computed previously.

As an illustration, we perform self-consistent ballistic transport calculations in the p-Si GAA MOSFET [Fig. 2(b)] at $T=300$ K in the sp^3s^* tight-binding model with the same lattice orientation and the wire cross section as in the previous example. Other parameters are: $\epsilon_{Si}=11.9$, $\epsilon_{SiO_2}=3.8$, dopant concentration in source/drain region 2×10^{19} cm^{-3}, and applied bias $V_{SD}=0.1$ V. Figure 4 presents an example of calculated I-V characteristics. The bottleneck of the calculations is the R-matrix propagation which in the present case (7040 Si atoms in total) takes ~ 10 s for each energy point on 3.2 GHz workstation. The computational time for the carrier density is negligible. The method clearly has no limitations to the device geometry and lattice orientation. As an extra test, we compute the drain current in 180 GAA MOSFETs with Si-surface roughness using the Gaussian model[19] with the correlation length 2 nm and the amplitude of one atomic layer. The distribution of I/I_0 (where I_0 is the current in the ideal MOSFET) for $V_G=-0.22$ V is shown in the inset of Fig. 4.

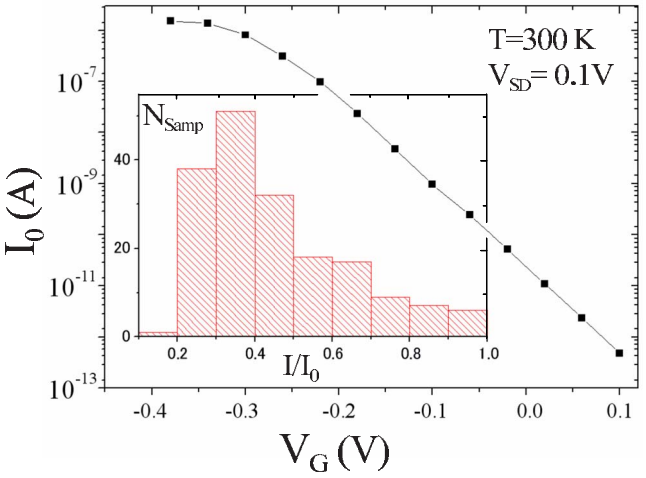

FIG. 4. (Color online) I-V characteristics of GAA MOSFET in Fig. 2(b). The inset shows the statistics of the current I at $V_G=-0.22$ V in 180 devices with silicon surface roughness.

Going beyond the ballistic approximation would require calculation of the whole Green's function. It is worth to note in this connection that the R-matrix propagation also gives enough information for recursive solution of the Dyson equation, Eq. (6). Figure 5 shows schematically one step of such calculations. Numeration of rows and columns in the device Green's function in this figure corresponds to the consecutive order of atoms in the device growth. For arbitrary cluster $\tilde{C}$ and known $P_{\tilde{B}}\mathbf{G}^R P_{\tilde{B}}$, the calculation of $P_{\tilde{C}}\mathbf{G}^R P_{\tilde{B}}$ is analogous to the wave function. In particular, one obtains $P_a\mathbf{G}^R P_{\tilde{B}}$ for the last atom a in $\tilde{C}$ [Fig. 5(a)]. When going to the previous cluster C, the only missing part of $P_B\mathbf{G}^R P_B$ is the diagonal term $\mathbf{G}^R_{aa}\equiv P_a\mathbf{G}^R P_a$ [Fig. 5(b)] which is calculated trivially from the Dyson equation with the bare Green's function $\frac{1}{\varepsilon-\mathbf{H}_{\tilde{C}\tilde{C}}}$,

$$\mathbf{G}^R_{aa} = \tilde{\mathbf{R}}_{aa} + \Theta_{a\tilde{b}}\mathbf{G}^{R^T}_{a\tilde{b}}. \tag{28}$$

The nondiagonal block $P_C\mathbf{G}^R P_a$ [Fig. 5(c)] is now treated as the wave function Ψ_C, which can be found by the backward propagation Eq. (25) since its value $\Psi_B\equiv P_B\mathbf{G}^R P_a$ outside

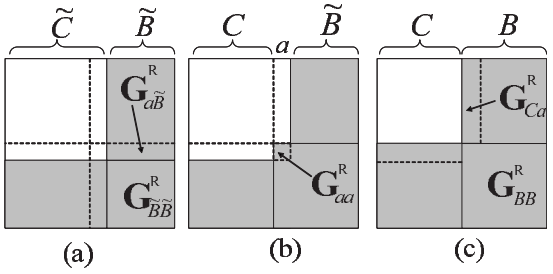

FIG. 5. Recursive integration of the Dyson equation. The calculated blocks of the Green's function are shown dark. (a) The nondiagonal block $\mathbf{G}^R_{a\tilde{B}}$ is a part of $\mathbf{G}^R_{\tilde{C}\tilde{B}}$ calculated from $\mathbf{G}^R_{\tilde{B}\tilde{B}}$ beforehand. (b) The diagonal block $\mathbf{G}^R_{aa}$ for the atom a is calculated by Eq. (28). (c) The nondiagonal block $\mathbf{G}^R_{Ca}$ (and therefore $\mathbf{G}^R_{aC}$) is calculated by the backward propagation Eq. (25).

the cluster C is known. Thus, the backward propagation of the full Green's function only requires the R-matrix component for the last atom $\tilde{\mathbf{R}}_{aa}$ to be stored in addition to $\Theta_{a\tilde{b}}$. The initial condition for the backward propagation is given by the Green's function at the contacts Eq. (10). Similar scheme is applicable to the Hamiltonians with local corrections due to inelastic phonon scattering in the Born approximation.[20] As a test, we have computed the full retarded Green's function in the GAA MOSFET in Fig. 2(b) at zero bias. We have directly checked each component in the matrix identity $\mathbf{G}^R(\varepsilon - \mathbf{H}_{\mathrm{DD}}) = \mathbf{1}$ away from the contacts and confirmed at least nine digits of accuracy. Since solving the Dyson equation is an extension of the wave-function calculations, this test brings extra confidence that our scheme for the ballistic regime is reliable.

IV. SUMMARY

In this paper we present the R-matrix method for atomistic quantum device simulations. Similar to the CBR scheme, the method utilizes the fact that the current carrying states in the open device can be found in terms of the Green's function of the corresponding close system. However, instead of dealing with the huge device Hamiltonian, we treat the device as a growing cluster of atoms which is reminiscent of the recursive Green's function method. The propagated quantity in our scheme is the R matrix defined as a boundary part of the Green's function in the close system. The device R matrix is related to the electric current through the contacts with leads and it can be calculated recursively in devices of arbitrary geometry. Such a propagation scheme is very stable, accurate, and it does not involve any huge operations. It is further shown that the R-matrix propagation simultaneously provides extra data which enables the Schrödinger and/or Dyson equations to be integrated in a straightforward way. The numerical examples demonstrate high numerical performance regardless of random impurities and the interface roughness.

ACKNOWLEDGMENT

This work was supported by Japan Science and Technology Agency.

*gena@si.eei.eng.osaka-u.ac.jp

[1] N. Lindert, L. Chang, Y. Choi, E. H. Anderson, W. Lee, T. King, J. Bokor, and H. Chenming, IEEE Electron Device Lett. **22**, 487 (2001).
[2] P. L. McEuen, M. S. Fuhrer, and H. K. Park, IEEE Trans. Nanotechnol. **1**, 78 (2002).
[3] J. Xiang, W. Lu, Y. Hi, Y. Wu, H. Yan, and C. M. Lieber, Nature (London) **441**, 489 (2006).
[4] H. R. Khan, D. Mamaluy, and D. Vasileska, IEEE Trans. Electron Devices **54**, 784 (2007).
[5] D. Mamaluy, D. Vasileska, M. Sabathil, T. Zibold, and P. Vogl, Phys. Rev. B **71**, 245321 (2005).
[6] H. Xu, Phys. Rev. B **50**, 8469 (1994); **50**, 12254 (1994).
[7] J. A. Torres and J. J. Saenz, J. Phys. Soc. Jpn. **73**, 2182 (2004).
[8] S. Rotter, J. Z. Tang, L. Wirtz, J. Trost, and J. Burgdörfer, Phys. Rev. B **62**, 1950 (2000).
[9] M. Luisier, A. Schenk, and W. Fichtner, J. Appl. Phys. **100**, 043713 (2006).
[10] G. Mil'nikov, N. Mori, Y. Kamakura, and T. Ezaki, J. Appl. Phys. **104**, 044506 (2008).
[11] U. Wulf, J. Kucera, P. N. Racec, and E. Sigmund, Phys. Rev. B **58**, 16209 (1998).
[12] T. Jayasekera, K. Mullen, and M. A. Morrison, Phys. Rev. B **74**, 235308 (2006).
[13] G. Mil'nikov, N. Mori, Y. Kamakura, and T. Ezaki, Phys. Rev. Lett. **102**, 036801 (2009).
[14] C. Rivas and R. Lake, Phys. Status Solidi B **239**, 94 (2003).
[15] C. Strahberger and P. Vogl, Phys. Rev. B **62**, 7289 (2000).
[16] S. Datta, *Electronic Transport in Mesoscopic Systems* (Cambridge University Press, Cambridge, England, 1995).
[17] P. Vogl, H. P. Hjalmarson, and J. D. Dow, J. Phys. Chem. Solids **44**, 365 (1983).
[18] S. Lee, F. Oyafuso, P. von Allmen, and G. Klimeck, Phys. Rev. B **69**, 045316 (2004).
[19] S. M. Goodnick, D. K. Ferry, C. W. Wilmsen, Z. Liliental, D. Fathy, and O. L. Krivanek, Phys. Rev. B **32**, 8171 (1985).
[20] R. Lake and S. Datta, Phys. Rev. B **45**, 6670 (1992).